Article

Journal of
Nanoscience and Nanotechnology
Vol. 19, 3816–3824, 2019
www.aspbs.com/jnn

A Comparative Analysis of ZnO Nanorods and Nanopencils Towards Amperometric Biosensing Applications

Mayoorika Shukla[1], Pramila[1], I. A. Palani[2], and Vipul Singh[1,*]

[1] *Molecular and Nanoelectronics Research Group (MNRG), Discipline of Electrical Engineering, Indian Institute of Technology Indore, Indore 453552, Madhya Pradesh, India*
[2] *Mechatronics and Instrumentation Lab, Discipline of Mechanical Engineering, Indian Institute of Technology Indore, Indore 453552, Madhya Pradesh, India*

In this work, ZnO Nanorods (ZNR) and Nanopencils (ZNP) were synthesized over Platinum (Pt) coated glass substrate by simple and low-temperature hydrothermal process for large-scale fabrication towards biosensing applications. The two types of morphologies have been obtained by using strong oxidizing agent viz $KMnO_4$ as an additive and replenishing the growth solution during the hydrothermal growth process. It was observed that incorporation of additive and replacement of growth solution has greatly influenced structural and electrochemical properties of ZNR/ZNP in terms of morphology, aspect ratio, and charge transfer hindrance. The aspect ratio has been found to increase by approximately three times from ZNR to ZNP which facilitated higher enzyme loading over ZNP as compared to ZNR. Moreover, electrochemical charge transport resistance was found to decrease by 36 times with changes in morphology and aspect ratio. Hence, significant variation in performance of as-fabricated enzymatic biosensor was observed. Amidst both the types of biosensors four-fold increment in sensitivity was found from ZNR to ZNP along with fast response time of 5s and a linear range of operation of 0.5–7.5 mM. The obtained results revealed that aspect ratio could be tuned efficiently by replacing the growth solution during hydrothermal growth which cognitively effects enzyme loading thereby influencing different figure of merits of the biosensor.

Keywords: Aspect Ratio, Enzyme, ZnO Nano-Pencils, Sensitivity, Biosensors.

1. INTRODUCTION

Miniaturization of the device in conjunction with high performance is a prerequisite for biosensors which have led to the utilization of nanomaterials for the same. A biosensor has been defined as an analytical device which consists of a bio-recognition element, i.e., a suitable support matrix immobilized with biomolecules (enzymes, DNA, antibody, etc.) attached to a transducer. The interaction between the bio-recognition element and analyte results in the generation of a signal which in turn is converted into electrical signal by transducer.[1,2] Nanomaterials have been explored exhaustively as bio-recognition element due to their high surface area and biocompatibility. The morphological variations obtained in reduced dimensions have a strong influence over the extent of immobilization, electrical and optical properties.[3] Especially 1-dimensional (1D) nanostructure based devices may result in innovative biological and physiological applications by probing local cellular environment due to quantum confinement at nano dimensions. Moreover, minimized diameters of the 1D nanostructure with dimensions comparable to individual biomolecule lead to detection at the single molecule level. One of the most suitable candidates for obtaining 1D nanostructures in reduced dimensions is semiconductor metal oxides like ZnO, SnO_2, and V_2O_5, etc.[4–7] Among different types of semiconductor metal oxides ZnO a wide band gap (E_g 3.3 eV at 300 K) II–VI compound which has received considerable interest due to its unique electrical and optical properties, a wide variety of nanostructures, non-toxicity, and biocompatibility.[8]

ZnO, a semiconductor with high exciton binding energy of 60 meV at room temperature[8] can be grown in a variety of morphologies such as nanorods, nanotubes, nanorings, nanosheets, nanoflowers, etc. by different physical

*Author to whom correspondence should be addressed.

 1533-4880/2019/19/3816/009 doi:10.1166/jnn.2019.16330

methods viz pulsed laser deposition, sputtering, spray pyrolysis, vapor deposition, etc. Furthermore, different types of nanostructures have been prepared by low-cost solution based approaches as well viz. sol–gel, electrochemical and hydrothermal, etc.[8–20] Amongst all these fabrication techniques hydrothermal growth process is a cost-effective, low-temperature method which facilitates large-scale fabrication of the device. Additionally, ZnO being biocompatible and having a high isoelectric point (IEP = 9.5) has led, towards its usage as an appropriate matrix for immobilization of biomolecules with retained and enhanced activity of biomolecules.[4, 15] The extent of immobilization of biomolecules plays a very crucial role in the performance of biosensors. Hence, many electrochemical enzymatic biosensors utilizing ZnO as a support matrix for detection of glucose, urea, phenol, and cholesterol, etc. have been explored immensely in the literature.[4, 16–17, 21–23] Enzymes are highly specific due to their high catalytic activity and thus being mainly employed for electrochemical detection. From these, glucose sensors are most widely explored biosensors, due to its exhaustive application in different fields ranging from biological and chemical analysis to environmental monitoring and clinical applications.[20] In this context, ZnO nanostructures have been explored exhaustively.[16, 21, 23–25] Kong et al. fabricated ZnO nanotubes by chemical etching of electrodeposited ZnO nanorods and employed the same for glucose detection.[16] Munje et al. have utilized RF-sputtered ZnO thin films deposited on flexible substrates for glucose and cortisol detection.[24] Ahmad et al. physically adsorbed GO_x over ZnO nanofiber and performed glucose detection.[21] Marie et al. have presented Glucose oxidase (GO_x) mediated detection of glucose using ZnO nanorods as a support matrix.[25] Generally, most of the reports emphasize mainly towards the fabrication of ZnO nanostructures separately followed by transfer of the nanostructures to the electrode which involves tedious additional steps and is quite cumbersome. Moreover, very few articles accentuate towards variation in morphology, geometry, shape and aspect ratio of nanostructures and its subsequent influence over biosensing applications.

In this work, an electrochemical enzymatic glucose biosensor has been analyzed with the aim of studying variations in morphology of ZnO nanostructures and its effect on aspect ratio thereby having an impact on enzyme loading and glucose biosensing. The morphological and aspect ratio variation was performed by merely replenishing the hydrothermal growth solution at different intervals with the *in-situ* addition of $KMnO_4$ as an additive which has led to the fabrication of ZNR and ZNP. Additionally, electrochemical and electrical properties were observed to improve along with enhancement in aspect ratio. The as-prepared ZNR and ZNP grew directly over the electrode were used as solid support for immobilization of GO_x by simple physical adsorption method. Finally, amperometric detection of glucose was performed, and it was observed to be influenced by aspect ratio and charge transfer resistance.

2. EXPERIMENTAL DETAILS

2.1. Reagents

Zinc Acetate, Ethanolamine, 2-methoxy ethanol, Zinc Nitrate ($Zn(NO_3)_2 \cdot 6H_2O$), Hexamethylenetetramine ($C_6H_{12}N_4$), $KMnO_4$, Sodium phosphate dibasic (Na_2HPO_4), Potassium phosphate monobasic (KH_2PO_4), NaCl, Uric acid, Ascorbic acid, Potassium ferricyanide/ferrocyanid $[Fe(CN)_6]^{-3/-4}$, Glucose oxidase from Aspergillus niger (E.C. 1.1.3.4) having specific activity of 166 U/mg as mentioned by manufacturer, D-(+)-glucose, Nafion (5 wt% in water and lower aliphatic alcohol) were used as procured from Sigma Aldrich. All chemicals were of analytical grade and used without any further purification. 0.01 M Phosphate buffered saline solution of pH 7.4 was prepared from KH_2PO_4 and Na_2HPO_4 with 0.137 mM NaCl. 1M glucose stock solution was prepared in De-ionized (DI) water and kept on stirring for 24 h for mutarotation, to establish equilibrium concentration between α and β anomers. DI water (>18 MΩ) obtained from Milli-Q purifying system was used for the preparation of all the aqueous solutions.

2.2. Synthesis of ZNR/ZNP

In the typical synthesis process, glass samples were cut into 1 cm × 1 cm size and cleaned by an ultra-sonication process in acetone, isopropyl alcohol, and DI respectively, followed by drying. After cleaning, 50 nm Pt was sputtered over the samples, at a base pressure of 2×10^{-6} mbar. Before Pt deposition, a 5 nm Cr layer was deposited to improve adhesion of Pt over the glass.[1] The samples have been rotated at a speed of 10 revolutions per minute (rpm) to ensure uniform deposition of Pt over it. Two types of morphologies were obtained by the hydrothermal growth process on Pt coated glass substrates. Figures 1(a)–(b) shows the schematic for the fabrication of ZnO nanostructures having different morphologies such as ZNR and ZNP. The Glass/Cr:Pt samples were pretreated to obtain a thin ZnO seed layer which provides sites for heterogeneous nucleation, as reported elsewhere.[26, 27] Briefly, seed solution of Zinc acetate (2M) and ethanolamine (2M) in 2-methoxy ethanol was prepared and spin coated over Glass/Cr:Pt samples, followed by annealing of the same. Afterward, pretreated samples were kept for the growth of ZnO nanostructures in an equimolar solution of Zinc nitrate and Hexamethylenetetramine (HMTA) with the *in-situ* addition of $KMnO_4$ (5 mM) as an additive. The $KMnO_4$ was utilized as an additive to obtain thin films of nanostructures with better adhesion towards the substrate. The two different types of morphologies were obtained without and with the replacement of solution at every 4 h i.e., ZNR (Fig. 1(a)) and ZNP (Fig. 1(b)), respectively. The hydrothermal growth was performed for 12 h at 110 °C.

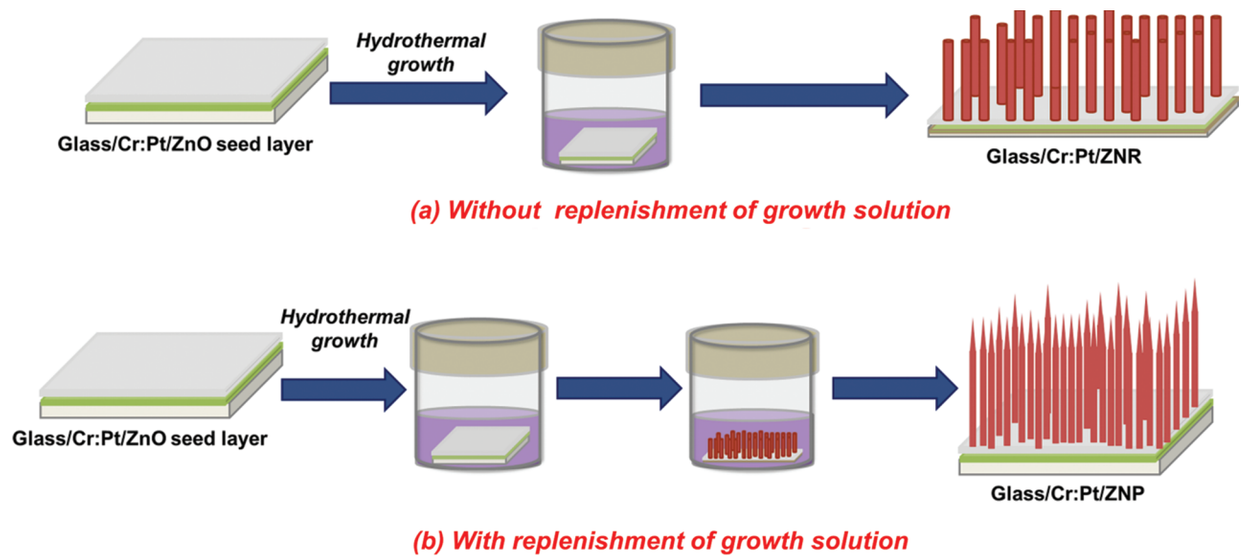

Figure 1. Schematic showing fabrication of (a) ZNR—Without replenishment of solution and (b) ZNP—With replenishment of solution.

Here, the solution was replaced with the aim of achieving high aspect ratio.[28] The as discussed growth process resulted in two types of nanostructures with varied aspect ratio. ZnO nano-dumbells (ZND) were obtained for 0 mM $KMnO_4$ concentration while 5 mM $KMnO_4$ concentration has resulted in the formation of ZNR or ZNP depending on replenishment of growth solution. ZNR were obtained after growth of 4 h which was performed without replenishment of growth solution whereas ZNP were formed after growth of 12 h with replenishment of growth solution at every 4 h. Finally, samples were cleaned thoroughly with acetone and DI to remove any residual salt present followed by drying.

2.3. Biosensor Fabrication, Enzyme Immobilization, and Quantification

The immobilization of enzymes i.e., attachment process of enzymes to the solid support matrix was performed via physical adsorption process.[29] It was utilized for the immobilization of enzymes over support matrix due to ease and simplicity of the technique. In this process, the high isoelectric point (IEP) of ZnO (IEP = 9.5) facilitates the immobilization GO_x (IEP = 4.5) via electrostatic binding.[26] Further, this process leads to the minimal changes in enzyme conformation. The GO_x was immobilized on ZNR and ZNP, by drop-casting a 5 μl solution of GO_x stock solution (20 mg/ml GO_x prepared in PBS) followed by incubation for 24 h. The area of the enzyme electrode was around 0.1 cm^2. The loosely adhered enzymes were washed out from the GO_x immobilized electrode with PBS after drying in an incubator. Further, 0.5% Nafion solution was drop cast over it and kept overnight for drying which prevents enzyme leaching from the electrode surface.[3] The as-prepared electrode was stored in the incubator at 4 °C, when not in use.

The amount of enzyme immobilized over ZNR and ZNP has been quantified by fluorescence. Tryptophan which is present in each GO_x molecule is an aromatic molecule and contributes to an intrinsic fluorescence in GO_x. Thus on excitation at 280 nm, GO_x molecules present in solution gives fluorescence emission at 330 nm. Therefore, the fluorescence emission intensity is proportional to the amount of GO_x present in the solution. The same property has been used here for determination of enzyme loading.[30] The amount of immobilized enzymes over the support matrix has been termed as enzyme loading. Further, to estimate enzyme loading the linear calibration curve was measured by recording steady-state fluorescence for a known amount of GO_x in PBS. Each electrode was cleaned in PBS before Nafion drop casting for removal of unadhered GO_x molecules from it. This PBS solution containing unadhered GO_x molecules was collected separately. After that, the fluorescence of this solution was recorded. Since 100 μg of GO_x has been immobilized on support matrix and the amount of loosely bound GO_x molecules can be determined by fluorescence intensity of collected solution and the calibration curve. Finally, enzyme loading could be determined merely by the subtraction of the amount of unadhered GO_x molecules from 100 μg.

2.4. Characterization and Measurement

The morphology of fabricated viz. ZNR and ZNP were analyzed by Field Emission Scanning Electron Microscopy (FESEM) i.e., Sigma Supra™ 55; Carl Zeiss. The distribution of length and diameter of ZNR and ZNP was obtained by using imtool of MATLAB.[26] The crystalline structure and phase transformations were analyzed by powder XRD (RigakuSmart Lab® System) with Cu Kα radiation operating at 40 kV and 40 mA, using Cu Kα radiation ($\lambda = 1.5418$ Å) in the 2θ range from 20° to 80°. The PL

spectrometer (Dongwoo Optron DM 500i) having an excitation source consisting of a continuous wave He–Cd laser (excitation wavelength, 325 nm, PMT detector) was used to measure the PL emission from the samples. Fluorescence emissions were obtained using FluoroMax-4p Spectrofluorometer from Horiba Jobin Yvon (Model: FM-100). Excitation and emission slit widths were set at 2 nm each, and the samples were excited at 280 nm. The frequency dependent impedance analysis was performed by electrochemical work station (Autolab PGSTAT 302N) using three-electrode cell configuration with Glass/Cr:Pt/(ZNR or ZNP), Ag/AgCl and Pt foil electrode as working, reference and counter electrode respectively. Furthermore, amperometric glucose biosensor response and cyclic voltammetry studies were performed by using similar three-electrode cell configuration and electrochemical work station with Glass/Cr:Pt/ (ZNR or ZNP)/GO_x/Nafion as working electrode.

3. RESULTS AND DISCUSSION

3.1. Surface Morphology and Structural Characterization

The morphology, shape, and geometry of hydrothermally grown ZnO nanostructures were observed to be driven by many factors like growth temperature, precursors, replenishing the solution, pH, etc. This ease in tuning the morphology of ZnO nanostructures has been utilized for aspect ratio variation from ZNR to ZNP. The surface morphology change in ZnO nanostructures, the effect of the addition of $KMnO_4$ and replenishment of solution over the surface morphology has been evaluated by FESEM images as shown in Figures 2(a)–(d). The ZnO microstructures with dumbbell-like appearance were formed in samples grown without the addition of $KMnO_4$ as reported in our previous work.[27] The clusters of twinned hexagonal microrods and aggregates of dumbbells with dimensions ranging from 2–6 μm were observed with the growth in all the directions. The formation of dumbbells and clusters of twinned hexagonal microrods in Zinc nitrate and HMTA growth solution has been explained in detail by Yu et al.[31] Figures 2(a) and (c) shows the top view while Figures 2(b) and (d) depicts cross-sectional view of the ZNR and ZNP respectively. It was evident from Figures 2(a)–(b) that for 4 h growth, performed without replacement of solution the nanostructures were found to be rod like in shape having evident hexagonal top facet. The nanorods were uniformly distributed over the entire substrate. ZNP covering the whole substrate were obtained by growth of 12 h with replenishment of growth solution at every 4 h, as visible from Figures 2(c)–(d). In hydrothermal growth, aspect ratio increases on increasing the growth time. But the growth rate slows down significantly after 4 h since reactant concentration, and precursor supersaturation decreases i.e., the nutrient solution becomes devoid of precursors due to homogeneous nucleation taking place in solution resulting in nearly same aspect ratio even after extended growth time.[28] Hence, to obtain enhanced aspect ratio growth solution has been replaced at every 4 h with a fresh precursor solution having same nutrient (Zinc Nitrate and HMTA) and additive ($KMnO_4$) concentration. Here in case of ZNP, the tapering of top face and morphology variation from rod to pencil can be attributed to the presence of an oxidizing agent in growth solution which leads to change in growth rate anisotropy of different planes on replacing the solution. Additionally, incorporation of $KMnO_4$ refrains the formation of $(CH_2)_6N_4$–$4H^+$ ions, ceasing the formation of dumbbells in the form of precipitates leading to uniform and powder free growth of ZNP.[28, 32–34]

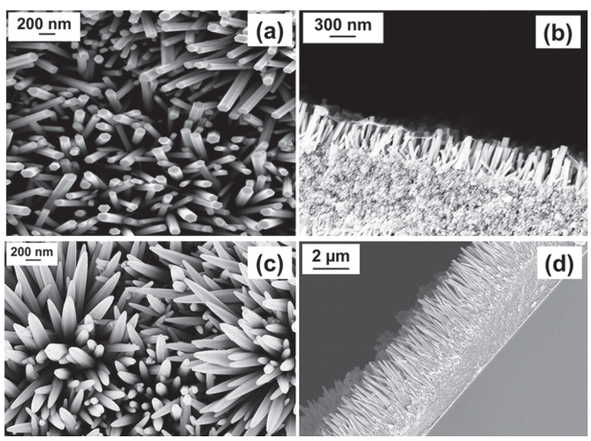

Figure 2. FESEM images showing of ZNR (a) top view, (b) cross-sectional view; ZNP (c) top view and (d) cross-sectional view.

Figures 3(a)–(d) shows the histogram plot of diameter and length distribution of ZNR and ZNP. The diameter distribution of both the electrodes was observed to vary from 120–170 nm while a drastic improvement in length was obtained from ZNR to ZNP viz. approximately 0.5 μm to 2.25 μm, respectively. In this context, different calculations of the average diameter and length distribution were performed using image processing toolbox of MATLAB as listed in Table I. The aspect ratio of ZNR was calculated as the ratio of average length to average diameter of nanorods whereas for ZNP it was computed to be the ratio of average length to the average bottom diameter.[35–37] There has been a threefold increment in aspect ratio from ZNR to ZNP. The aspect ratio was found to increase to 13 from 4.4 by a simple modification in the growth method since average length has increased almost five times.

The XRD pattern for as prepared ZNR and ZNP grew with 5 mM additive concentration has been shown in Figure 4(a). The fabricated ZNR and ZNP samples were found to have diffraction peaks at 31.7°, 34.4°, 36.3°, 47.5°, 56.6°, 62.9° and 69.1° corresponding to ZnO wurtzite phase (space group P63mc, JCPDS–36-1451) (100), (002), (101), (102), (110), (103) and (112) with an extra peak at $2\theta = 40°$ indexed to Pt coated over glass

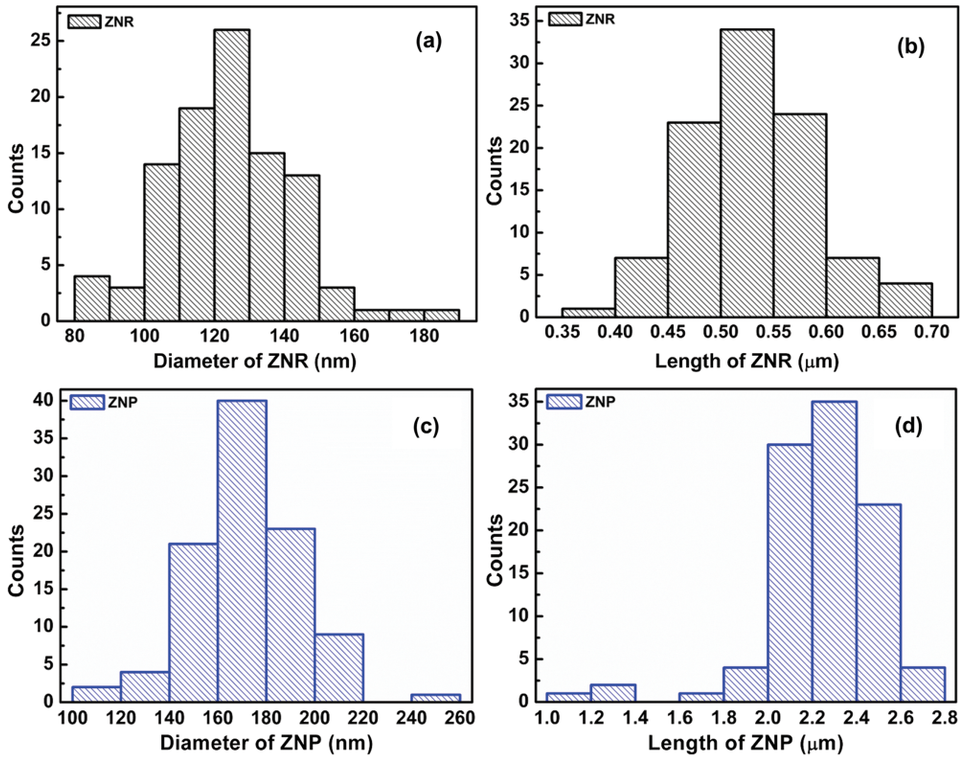

Figure 3. Histogram plot for ZNR (a) diameter distribution, (b) length distribution; ZNP (c) diameter distribution and (d) length distribution of randomly selected 100 nanorods and nano pencils from corresponding FESEM images.

substrate. The as-prepared ZnO was pure as no peak other than ZnO wurtzite phase was recorded; signifying towards the absence of any impurity in the sample or intermediate formation during growth, within the detection limit of the instrument. The intense peaks of diffraction confirm the high degree of crystallization of different types of nanostructures. The massive enhancement in the intensity of (002) peak has been observed from ZNR to ZNP as depicted in Figure 4(a), which indicates towards oriented growth. Furthermore highly pronounced (002) peak indicates towards the vertical orientation of nano-pencils.

The main factors responsible for the formation of ZNP were the replenishment of growth solution which eventually led to the sudden supply of nutrient around the nanorods and presence of $KMnO_4$ as an additive. The addition of $KMnO_4$ in the nutrient solution provides an oxygen rich environment which acts as a driving force for anisotropic growth along *c*-axis and supply of more OH^- ions by promoting the hydrolysis of HMTA.[27]

Table I. Aspect ratio of two different type of electrodes with average length and diameter distribution.

ZnO sample	Average diameter (nm)	Average length (μm)	Aspect ratio
ZNR	120	0.53	4.4
ZNP	170	2.25	13

The morphology of nanostructures depends on the growth rate of slowest growing nonpolar planes. The fastest growing polar plane is prone to disappearance[32, 33, 38] which has been observed from FESEM images of ZNP leading to the formation of nano-pencils. Figure 4(b) shows the schematic of morphology modulation from nanorod to nano-pencil.

3.2. Electrochemical Impedance Spectroscopy

Further, electrochemical impedance spectroscopy (EIS) was performed to investigate the electron transfer capability and electrical properties at the electrode-electrolyte interface of as prepared electrodes. The frequency distribution data which shows electron transfer at the electrode-electrolyte interface was obtained by application of an AC signal. The EIS spectra show the Nyquist plot which consists of a semicircle and a Warburg line with unity slope at high and low frequencies, respectively. The Nyquist plot comprises of four parts; the ohmic resistance of electrolyte solution, Warburg impedance, double layer capacitance and the electron transfer resistance.[39] The semicircle obtained at high frequencies represents the electron transfer kinetics of redox mediator, and its diameter is equal to charge transfer resistance (R_{ct}) while Warburg depends on mass diffusion properties of the redox probe in the electrolyte solution. The numerical value of R_{ct} of as prepared nanostructures can be calculated by the diameter of

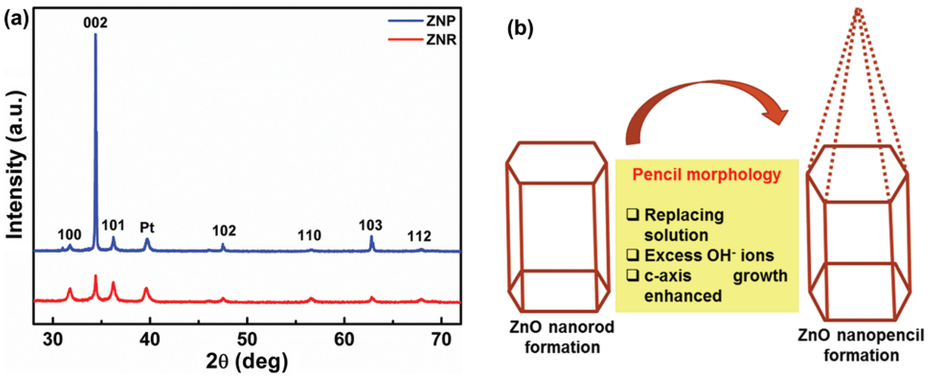

Figure 4. (a) XRD pattern for obtained ZnO nanostructures; (b) schematic showing ZNR to ZNP conversion.

semicircle observed in Nyquist plot.[40] The EIS spectra of Glass/Cr:Pt/(ZNR or ZNP) electrodes has been obtained using electrolyte solution of 5 mM $[Fe(CN)_6]^{-3/-4}$ (redox mediator) in 0.1 M KCl (supporting electrolyte), by application of an alternating voltage of 10 mV. The frequency was swept from 10 kHz to 0.1 Hz. Figure 5 shows the Nyquist plot corresponding to hydrothermally grown ZnO electrodes. There was a significant improvement in charge, and mass transfer properties from ZNR to ZNP since a clear semicircle and Warburg line was present in the Nyquist plot for ZNP unlike only a semicircle for ZNR. The inset of Figure 5 shows the Nyquist plot for bare Pt electrode and equivalent circuit model utilized for fitting. The fitted equivalent circuit for the electrochemical system was Randle's model which consists of solution resistance (R_s) in series with the parallel combination of charge transfer resistance (R_{ct}), Warburg resistance (W) and double layer capacitance (C). The resistance W corresponds to the diffusion properties while the capacitance C represents the electrode interface with the electrolyte and is indicative of the properties like roughness and inhomogeneity. The R_{ct} represents the electrical property of the film under study and is inversely proportional to the rate of charge transfer through the film. The value of R_s and R_{ct} has been

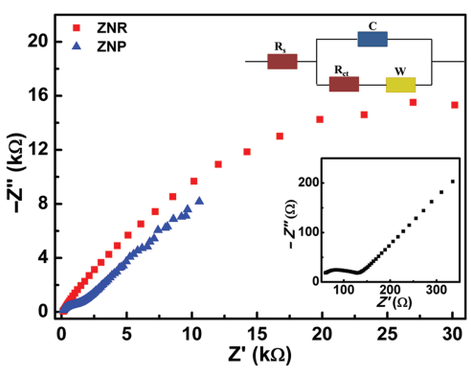

Figure 5. The Nyquist plot of as-fabricated ZNR and ZNP electrodes. The inset of the same shows the Nyquist plot for bare Pt electrode and equivalent circuit model utilized for fitting.

determined by fitting Nyquist plot data using Z_{sim} program software.[26] The R_s was obtained to be around 80 Ω. The R_{ct} values obtained for different electrodes suggest a major difference in charge transfer behavior with morphological variations. The R_{ct} for ZNR was calculated to be 55 KΩ which indicates towards huge hindrance in charge transfer near the electrode-electrolyte interface. However, in the case of ZNP semicircle diameter tends to decrease significantly to 1500 Ω. The 36 fold decrease in electrochemical charge transfer resistance and improvement in the electrical properties of the electrode has been attributed to enhanced aspect ratio and change in shape of nanostructures from ZNR to ZNP.

3.3. Enzyme Quantification

The enzyme loading, i.e., amount of enzyme immobilized on support matrix has been determined by recording the fluorescence intensity variation in GO_x molecules. The average length of ZNP was found to increase by five times as compared to ZNR. Hence, the aspect ratio was observed to be 4.4 for ZNR while it was calculated to be 13 for ZNP. Enzyme loading majorly depends on the surface to volume ratio available for immobilization of enzymes. Thus, it was found to vary with aspect ratio. Moreover, the morphology of ZNP with nanotip like ending enhances the extent of immobilization.[33] The threefold enhancement in aspect ratio from ZNR to ZNP was responsible for the direct doubling of enzyme loading i.e., from 444 μg-cm^{-2} in ZNR to 800 μg-cm^{-2} in ZNP. Additionally, GO_x enzyme has an active center unit, i.e., Flavin Adenine Dinucleotide (FAD) which is buried deep in the outer protein shell. The FAD active center participates in the oxidation of glucose. The morphology such as ZNP with nanotips ending help in exposing out these FAD units from protein shells, which in turn influences the biosensor response.

3.4. Biosensor Characterization

3.4.1. Amperometric Response

The three electrode cell configuration with Glass/Cr:Pt/ZNR or ZNP/GO_x/Nafion, Ag/AgCl and Pt foil as

working, reference and counter electrode respectively were employed for biosensor characterization. PBS with 0.01 M concentration and pH = 7.4 was used as an electrolyte solution. Current response measurement was performed for both the electrodes utilizing ZNR and ZNP as the support matrix for immobilization of GO_x. The glucose aliquots added to the electrolyte solution were detected amperometrically by applying the constant potential to the working electrode. GO_x immobilized over support matrix oxidizes glucose into gluconic acid and gets itself reduced which is again oxidized by oxygen present in solution releasing H_2O_2 as a byproduct. This H_2O_2 is detected by application of potential and gives a measure of glucose added to the solution shown in Eqs. (1)–(3).

$$C_6H_{12}O_6 + GO_x(FAD) + H_2O \rightarrow C_6H_{12}O_7 + GO_x(FADH_2) \quad (1)$$

$$GO_x(FADH_2) + O_2 \rightarrow GO_x(FAD) + H_2O_2 \quad (2)$$

$$H_2O_2 \xrightarrow{0.8\ V} 2H^+ + 2e^- + O_2 \quad (3)$$

Current density increases upon injection of glucose due to the generation of electrons. The relationship between steady-state current density and the glucose concentration injected into the electrolyte solution was represented by the calibration curve. The typical nature of enzyme kinetics consists of a linear and saturation region. Initially, at lower concentrations of glucose, the current increases instantaneously on the addition of glucose since active sites of enzymes were unoccupied resulting in a linear region of the calibration curve. While at higher concentrations all the active sites get occupied by glucose molecules eventually heading towards saturation and thus there is no further increase in current density on injection of glucose after saturation. Hence calibration curves obtained from amperometric response consists of two regions; linear and saturation region. The linear region gives a measure of the linear range of operation, and the slope of the same has been utilized to estimate the sensitivity of a biosensor.

The amperometric responses have been recorded for the two types of electrodes i.e., ZNR and ZNP at an applied potential of 0.8 V in a continuously stirred PBS of pH 7.4. ZnO is an amphoteric compound and therefore is stable around neutral pH. Moreover, pH of the blood is around 7.4, and thus the same value was chosen for all the biosensor characterizations. Figure 6 shows the typical step like amperometric response for both the types of electrodes. The glucose aliquots have been added to the continuously stirred electrolyte solution in an interval of 30 s. An immediate rise in current density has been observed for the two different types of electrodes on the subsequent addition of glucose as clear from Figure 6. Response time was defined as the time taken by current density to increase up to 90% of steady state value after addition of glucose. It was determined to be 5–6 s with a variable linear range and sensitivity for ZNR and ZNP electrodes. The fluctuations in

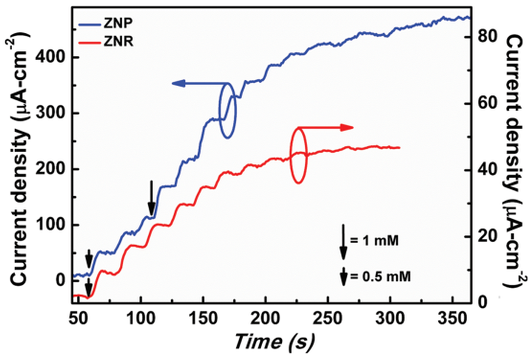

Figure 6. The amperometric response of current density variation viz. time for ZNR and ZNP biosensor electrodes.

the current density with respect to time are observed due to the mechanical stirring which has been performed to provide convective transport. Further, Figure 7 shows the calibration curve for the as-prepared biosensor electrodes which have been obtained from corresponding amperometric responses. The calibration curves obtained were in good agreement with the described enzyme kinetics having linear and saturation region. It implies that enzymes were appropriately immobilized over ZNR and ZNP support matrix with retained activity. The linear range was found to improve significantly from ZNR to ZNP electrodes. It is interesting to note that increment in aspect ratio from ZNR to ZNP has led to nearly four times increment in sensitivity i.e., 12.5 mA-cm^{-2}-M^{-1} for ZNR which has increased to 50 mA-cm^{-2}-M^{-1} for ZNP. The sensitivity of a biosensor was found to depend mainly on enzyme loading and charge transfer resistance; thus significant enhancement in performance of biosensor can be assigned to three-fold increment in aspect ratio and a decrease of 36 times in magnitude of R_{ct}. ZNP has shown substantial improvement in biosensor performance due to enhanced aspect ratio and higher enzyme loading (800 μg-cm^{-2}) with drastically reduced R_{ct}. The different figure of merits of the as-prepared biosensors have been tabulated and compared with some recently reported

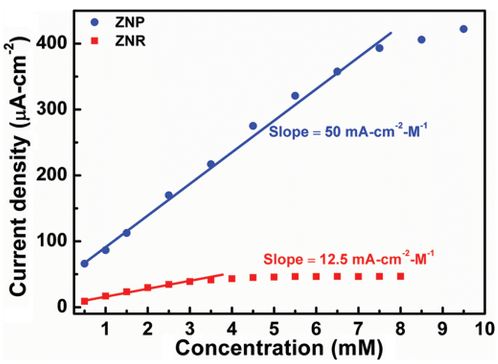

Figure 7. Calibration curve showing a comparison of the two types of biosensor electrodes.

work where ZnO nanostructures were utilized as a support matrix in Table II. The as-fabricated biosensor was found to outperform over other reported ZnO nanostructures such as nanoflowers, nanorods, mesoporous film, and nanotubes etc.[4, 16, 23, 41]

3.4.2. Cyclic Voltammetry Study

Furthermore to evaluate and compare the performance of the as-fabricated biosensors Cyclic Voltammograms (CV) were analyzed to study GO_x mediated oxidation of glucose. Figure 8 shows CV which was executed in an unstirred PBS solution at a scan rate of 100 mV/s. The potential was swept from −0.2 V to 0.8 V versus Ag/AgCl, first in the absence and then in the presence of 1 mM glucose for both the type of electrodes i.e., Glass/Cr:Pt/ZNR/GO_x and Glass/Cr:Pt/ZNP/GO_x. An increase in the anodic current has been observed in the presence of 1 mM glucose as compared to the background in the absence of it for both the electrodes. A huge difference in the anodic current value was observed for ZNP in comparison with the slight change in case or ZNR which can be attributed to the enhanced enzyme loading and for ZNP type of electrodes. The significant improvement in anodic current further affirms the fact that immobilization and electron transfer was greatly improved in ZNP which is in good accordance with fluorescence and EIS studies. The CV investigations also validated findings obtained from the amperometric current response and enzyme-mediated oxidation of glucose.

3.4.3. Interference Effect and Storage Stability Study

The human blood and serum consist of many electroactive species other than glucose such as Uric acid, Ascorbic acid, etc. which may interfere with the biosensor performance while detection of glucose. Thus for obtaining a practical glucose biosensor, it is necessary to evaluate anti-interference ability of biosensor. Although incorporation of enzymes itself brings selectivity in the biosensor, still these species may affect accurate detection of glucose. Hence, the anti-interference capability of the best performing electrode, i.e., ZNP was examined by initially injecting 5 mM glucose in the electrochemical cell setup followed by addition of 0.1 mM Ascorbic acid and 0.4 mM Uric acid

Table II. Comparison of as fabricated ZNR and ZNP electrodes with recently reported works.

S. no.	Support matrix	Sensitivity ($mA\text{-}cm^{-2}\text{-}M^{-1}$)	Linear range (mM)	Response time (s)	Ref.
1	ZNP	50	0.5–7.5	5	This work
2	ZNR	12.5	0.5–3.5	6	This work
3	ZnO nanoflowers	41.13	0.01–5.2	5	[41]
4	ZnO nanorods	25.7	0.01–0.7	2	[23]
5	Mesporous ZnO	–	0.2–12	3	[4]
6	ZnO nanofibers	70.2	0.25–19	4	[21]
7	ZnO nanotubes	21.7	0.5–12	3	[16]

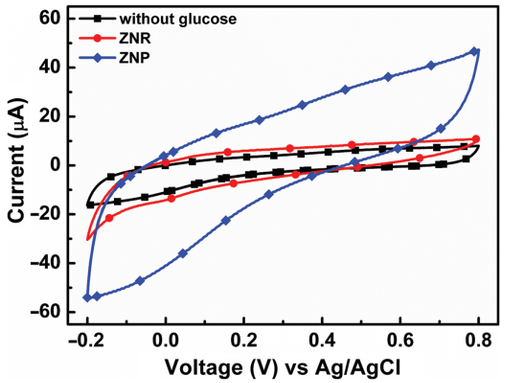

Figure 8. Cyclic voltammograms of the as-prepared electrodes without glucose and with an injection of 1 mM glucose.

sequentially. The concentration of these two species was kept same as present in physiological conditions (human blood).[21] Figure 9 shows the anti-interference capability for ZNP electrodes. An immediate rise in current density was observed on addition of 5 mM glucose while a sluggish increase of 1.3% and 1.57% was observed for ascorbic acid and uric acid addition as shown in Figure 9. The selectivity of biosensor and anti-interference capability can be attributed to enzymes which are highly specific towards its substrate and well immobilized over support matrix.

Moreover, to evaluate the stability of discussed biosensor for practical applications, the shelf life measurement was performed. The amperometric response has been recorded for ZNP after storing it for 7 days in an incubator at 4 °C. The step-like amperometric response was obtained with a minimal decrease of 4 $mA\text{-}cm^{-2}\text{-}M^{-1}$ in sensitivity which implies that biosensor has retained 92% of its initial sensitivity. The sensitivity of the biosensor was observed to decrease further on increasing the storage time to 15 days which can be attributed to leaching and denaturation of enzymes from the electrode with time.

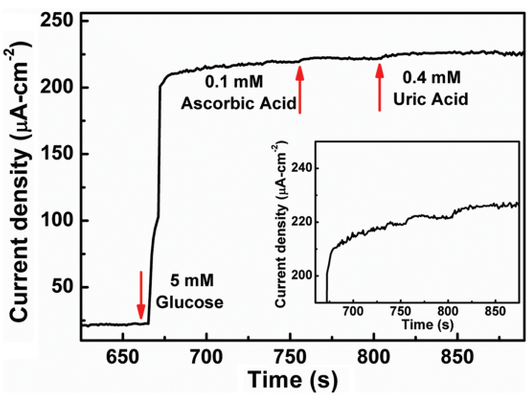

Figure 9. Interference effect study on biosensor response of ZNP electrode.

4. CONCLUSIONS

In summary, a novel and straightforward method of replacing the growth solution during hydrothermal growth process with the *in-situ* addition of $KMnO_4$ was employed for obtaining different morphologies of ZnO. ZNR and ZNP electrodes with morphological variations suitable for biosensing platform were obtained. Highly crystalline ZnO nanostructures with different aspect ratio were attained for evaluating the biosensor performance. The biosensor figures of merits were found to improve dramatically due to changes in aspect ratio leading to enhancement in enzyme loading and 36 times decrement in charge transfer resistance. The variation in morphology was responsible for three times improvement in aspect ratio by replenishing the growth solution which in turn was responsible for doubling of enzyme loading and leading to four times increase in sensitivity. Biosensor with higher aspect ratio and enzyme loading along with reduced R_{ct} i.e., ZNP was found to outperform with sensitivity, response time and linear range to be 50 mA-cm^{-2}-M^{-1}, 5 s, and 0.5–7.5 mM. The sensitivity was found to be strongly dependent on the surface to volume ratio available for immobilization of enzymes. Furthermore, morphology variations like nanotip endings have facilitated better enzyme loading. Thus the parameters influencing the morphology of ZnO during growth must be well optimized and explored to gain a better understanding about the process, which may also enable us to obtain high aspect ratio nanostructures facilitating higher enzyme loading and repression of R_{ct} thereby leading to high-performance biosensors.

Acknowledgments: One of the authors Mayoorika Shukla is grateful to FESEM, XRD, PL, Fluorescence, and Potentiostat/Galvanostat facilities equipped at the Sophisticated Instrument Centre, IIT Indore. Mayoorika Shuklawould also like to thank Dr. M. Anabarasu (Associate Professor, Discipline of Electrical Engineering, IIT Indore, Indore (M.P.), India) for the usage of the DC-RF magnetron sputtering system. She would like to thank Dr. P. M. Shirage (Associate Professor, Metallurgical Engineering, and Material Science, IIT Indore, Indore (M.P.), India) for providing access to EIS characterization facility. Mayoorika Shukla would further like to thank the Ministry of Human Resource and Development (MHRD), India for providing the Teaching Assistantship (TA). Author, Vipul Singh would like to thank the director of IIT Indore for providing his constant support and encouragement for research.

References and Notes

1. P. A. Palod and V. Singh, *Sens Actuators B Chem.* 209, 85 (**2015**).
2. M. A. Shiryaev, S. A. Eremin, and A. N. Baranov, *Nanotechnol. in Russia* 9, 99 (**2014**).
3. J. Li, H. Hu, H. Li, and C. Yao, *J. Mater. Sci.* 52, 10455 (**2017**).
4. M. Zhao, J. Huang, Y. Zhou, Q. Chen, X. Pan, H. He, and Z. Ye, *Biosens. Bioelecs.* 43, 226 (**2013**).
5. P. R. Solanki, A. Kaushik, V. V. Agrawal, and B. D. Malhotra, *NPG Asia Mater.* 3, 17 (**2011**).
6. H. Li, S. Liu, Z. Dai, J. Bao, and X. Yang, *Sensors* 9, 8547 (**2009**).
7. D. Panda and T. Y. Tseng, *J. Mater. Sci.* 48, 6849 (**2013**).
8. A. Janotti and C. G. Van de Walle, *Rep. Prog. Phys.* 72, 1 (**2009**).
9. Z. L. Wang, *Mater. Today* 7, 26 (**2004**).
10. Z. R. Tian, J. A. Voigt, J. Liu, B. Mckenzie, M. J. Mcdermott, M. A. Rodriguez, H. Konishi, and H. Xu, *Nat. Mater.* 2, 821 (**2003**).
11. T. Ma, M. Guo, M. Zhang, Y. Zhang, and X. Wang, *Nanotechnology* 18, 1 (**2007**).
12. T. Dixit, I. A. Palani, and V. Singh *J. Mater Sci: Mater. Electron.* 26, 821 (**2015**).
13. P. Rajagopalan, V. Singh, and I. A. Palani, *Mater. Res. Bull.* 84, 340 (**2016**).
14. A. Ali, S. Ambreen, R. Javed, S. Tabassum, I. U. Haq, and M. Zia, *Mater. Sci. Eng. C* 74, 137 (**2017**).
15. P. V. Morais, V. F. Gomes, A. C. A. Silva, N. O. Dantas, M. J. Schoning, and J. R. Siqueira Jr., *J. Mater. Sci.* 52, 12314 (**2017**).
16. T. Kong, Y. Chan, Y. Ye, K. Zhang, Z. Wang, and X. Wang, *Sens. Actuators B Chem.* 138, 344 (**2009**).
17. S. P. Singh, S. K. Arya, P. Pandey, B. D. Malhotra, S. Saha, K. Sreenivas, and V. Gupta, *Appl. Phys. Lett.* 9, 11 (**2007**).
18. A. Bilgaiyan, T. Dixit, G. Kapil, S. S. Pandey, S. Hayase, I. A. Palani, and V. Singh, *J. Nanosci. Nanotechnol.* 16, 3301 (**2016**).
19. A. Kumar, T. Dixit, I. A. Palani, D. Nakamura, M. Higashihata, and V. Singh, *Physica E* 93, 97 (**2017**).
20. A. Bilgaiyan, T. Dixit, I. A. Palani, and V. Singh, *Physica E* 86, 136 (**2017**).
21. M. Ahmad, C. Pan, Z. Luo, and J. Zhu, *J. Phys. Chem. C* 114, 9308 (**2010**).
22. M. Tak, V. Gupta, and M. Tomar, *Mater. Sci. Eng. C* 5, 738 (**2015**).
23. J. Zhao, D. Wu, and J. Zhi, *Bioelectrochemistry* 75, 44 (**2009**).
24. R. D. Munje, S. Muthukumar, and S. Prasad, *Sens. Actuators B Chem.* 238, 482 (**2017**).
25. M. Marie, S. Mandal, and O. Manasreh, *Sensors* 15, 18714 (**2015**).
26. M. Shukla, Pramila, T. Dixit, R. Prakash, I. A. Palani, and V. Singh, *Appl. Surf. Sci.* 422, 798 (**2017**).
27. T. Dixit, A. Bilgaiyan, I. A. Palani, D. Nakamura, T. Okada, and V. Singh, *J. Sol-Gel Sci. Technol.* 75, 693 (**2015**).
28. J. B. Baxter, A. M. Walker, K. Ommering, and E. S. Aydil, *Nanotechnol.* 17, S304 (**2006**).
29. P. A. Palod, S. S. Pandey, S. Hayase, and V. Singh, *Appl. Biochem. Biotechnol.* 174, 1059 (**2014**).
30. P. A. Palod and V. Singh, *Mater. Sci. Eng. C* 55, 420 (**2015**).
31. Q. Yu, C. Yu, H. Yang, W. Fu, L. Chang, J. Xu, R. Wei, H. Li, H. Zhu, M. Li, and G. Zou, *Inorg. Chem.* 466, 204 (**2007**).
32. L. Shi, A. J. T. Naik, J. B. M. Goodall, C. Tighe, R. Gruar, R. Binions, I. Parkin, and J. Darr, *Lang.* 29, 10603 (**2013**).
33. Q. Ahsanulhaq, A. Umar, and Y. B. Hahn, *Nanotechnol.* 18, 115603 (**2007**).
34. T. Dixit, I. A. Palani, and V. Singh, *J. Phys. Chem. C* 121, 3540 (**2017**).
35. R. Ahmada, N. Tripathya, and Y. B. Hahna, *Sens. Actuators B Chem.* 169, 382 (**2012**).
36. X. Liang, L. Shu, H. Lin, M. Fang, H. Zhang, G. Dong, S. Yip, F. Xiu, and J. C. Ho, *Sci. Rep.* 6, 341391 (**2016**).
37. H. Lin, F. Xiu, M. Fang, S. Yip, H. Y. Cheung, F. Wang, N. Han, K. S. Chan, C. Y. Wong, and J. C. Ho, *ACS Nano* 8, 3752 (**2014**).
38. R. C. Wang, C. P. Liu, J. L. Huang, S. J. Chen, Y. K. Tseng, and S. C. Kung, *Appl. Phys. Lett.* 87, 013110 (**2005**).
39. A. Kumar, M. Tiwari, and R. Prakash, *Chem. Electro. Chem.* 2, 2001 (**2015**).
40. Y. M. Lee and M. R. Zheng, *Appl. Surf. Sci.* 285P, 241 (**2013**).
41. B. Fang, C. Zhang, G. Wanga, M. Wanga, and Y. Jia, *Sens. Actuators B Chem.* 155, 304 (**2011**).

Received: 13 April 2018. Accepted: 14 May 2018.